Spiral patterns in oscillated granular layers

John R. de Bruyn*
Department of Physics and Physical Oceanography, Memorial University of Newfoundland, St. John's, Newfoundland, Canada A1B 3X7

B. C. Lewis, M. D. Shattuck, and Harry L. Swinney
Center for Nonlinear Dynamics and Department of Physics, University of Texas, Austin, Texas 78712
(Received 31 October 2000; published 28 March 2001)

Cell-filling spiral patterns are observed in a vertically oscillated layer of granular material when the oscillation amplitude is suddenly increased from below the onset of pattern formation into the region where stripe patterns appear for quasistatic increases in amplitude. These spirals are transients and decay to stripe patterns with defects. A transient spiral defect chaos state is also observed. We describe the behavior of the spirals, and the way in which they form and decay. Our results are compared with those for similar spiral patterns in Rayleigh-Bénard convection in fluids.

DOI: 10.1103/PhysRevE.63.041305 PACS number(s): 45.70.Qj, 45.70.Mg, 47.54.+r, 45.70.−n

I. INTRODUCTION

Granular materials appear simple: they consist of a large number of particles that interact solely through contact forces. While the physics of a single inelastic collision between two particles is conceptually straightforward, the collective dynamics of many particles, driven away from equilibrium and undergoing many inelastic collisions, is surprisingly rich and in many cases strongly nonintuitive. A variety of interesting phenomena occurring in granular materials has been studied recently, including convective flows in granular layers, heaping instabilities, force chains, and front propagation [1,2].

One of the most interesting types of collective behavior seen in granular materials is the pattern formation that results when a layer of granular material is oscillated vertically [3–16]. Patterns of stripes, squares, and hexagons are observed, depending on the frequency and amplitude of the oscillation [6]. Localized structures called oscillons are also observed [9]. The patterns seen in experiments have been reproduced in event-driven molecular-dynamics simulations of the oscillated granular system [13,14,17].

A variety of theoretical models of granular pattern formation have been introduced that capture the dynamics of the system to a greater or lesser degree [18–24]. This instability in an oscillating granular layer is analogous in many ways to the Faraday instability of an oscillated liquid layer, and an analysis similar to that for the Faraday instability has been performed for the oscillated granular layer, using equations derived from the kinetic theory of inelastic spheres [25,26]. Experiments and simulations have shown that the instabilities of stripe patterns in vertically oscillated granular materials are the same as those seen in fluid systems, suggesting that a continuum description analogous to the Navier-Stokes equation of fluid dynamics can be applied to vibrated granular layers [14].

Pattern formation in vibrated granular materials was observed by Fauve *et al.* in a quasi-two-dimensional system [3], and by Thomas *et al.* [4] in a three-dimensional system. Umbanhowar, Melo, and Swinney carried out a detailed study of the patterns which formed in a vertically vibrated layer of bronze spheres [6,9,12,16]. Their experimental system [10], a modified version of which is used in the present work, consisted of an evacuated cell containing a layer of granular material that was oscillated vertically by an electromagnetic shaker. The relevant experimental parameters are the amplitude of the sinusoidal acceleration Γ, measured in units of g, the acceleration due to gravity, the frequency of vibration f, and N, the depth of the granular layer in units of the particle diameter d. For low Γ, the granular layer simply moves up and down with the bottom plate of the cell. When Γ becomes greater than 1, however, the layer leaves the bottom plate for a portion of its cycle. The energy imparted to the layer by the bottom plate is dissipated in numerous collisions between particles, and between particles and the bottom plate. The layer becomes somewhat dispersed while in free fall, but overall it remains flat with uniform thickness. As Γ is increased through $\Gamma_c \approx 2.8$, there is a subcritical bifurcation at which a pattern of ''hills'' and ''valleys'' appears in the layer. For low f, the layer develops a pattern of squares, while for higher f, stripes appear [6,16]. When Γ is then decreased, the pattern vanishes at a value of Γ lower than Γ_c. The crossover from squares to stripes occurs at $f \approx 0.35/(g/Nd)^{1/2}$ [13]. These patterns are subharmonic, that is, the repeat time of the patterns is twice the period of the driving. The stripe or square patterns remain stable up to $\Gamma \approx 4$, at which point they lose stability to a hexagonal pattern. Period-2 flat layers and period-4 stripes and squares are observed at higher Γ. In the present paper we will be working in the region in which period-2 stripe patterns occur; the pattern formation ''phase diagram'' as a whole is discussed in Refs. [6,16].

In this paper we present experimental results on spiral patterns that form in a vertically oscillated granular layer in a range of driving amplitudes and frequencies. Large cell-filling spirals, isolated smaller spirals, and a state of spiral defect chaos [27] are all observed, depending on the experimental parameters. The existence of spiral patterns in vibrated granular layers has been noted briefly elsewhere

*Email address: jdebruyn@physics.mun.ca

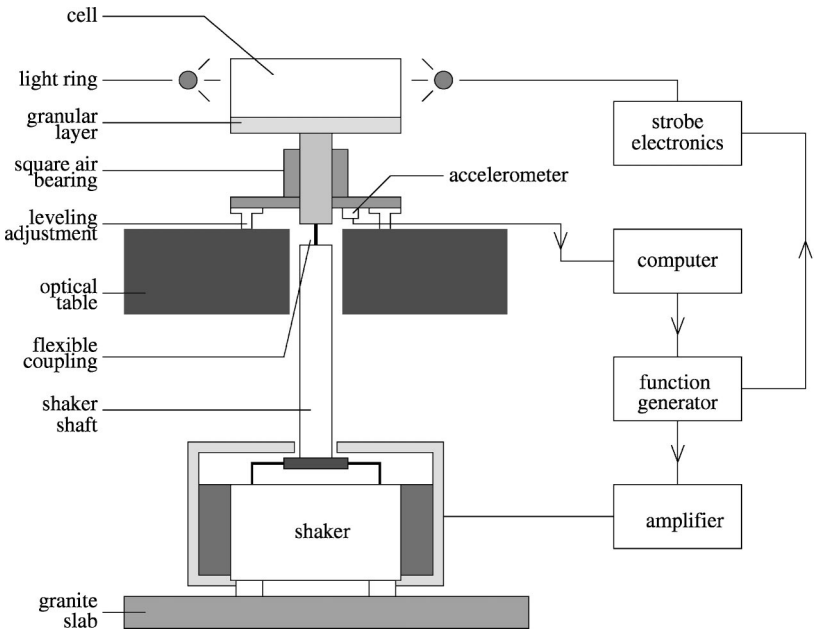

FIG. 1. A schematic diagram of the experimental apparatus, described in detail in the text.

[10,12]. Here we present a systematic survey of the range of parameters over which the spiral patterns exist, and discuss their dynamics in some detail. Similar spiral patterns have been studied in Rayleigh-Bénard convection in fluids; Ref. [28] is a recent review. Target and spiral patterns have also been observed in experiments on the Faraday instability [29].

The remainder of this paper is organized as follows. Section II contains a description of our experimental setup and techniques. Our results are presented in Sec. III and are discussed in Sec. IV. Section V is a brief conclusion.

II. EXPERIMENT

Our experimental apparatus is similar to that used in previous work [6,9,10,12,14,16]. It is shown schematically in Fig. 1. The cell containing the granular layer was shaken vertically by an electromagnetic shaker. Considerable effort was taken to ensure that the cell was driven accurately vertically, and to eliminate vibrations transmitted to the cell assembly by other than the shaker shaft. The shaker was mounted inside a housing which was filled with bags of lead shot. This housing was supported by leveling screws resting on an aluminum plate, which in turn sat on a granite slab resting on the laboratory floor. The shaker was driven by a sinusoidal voltage at a frequency f produced by a function generator and amplified by a power amplifier. The shaker drove a hardened steel shaft which was connected by a flexible coupling to a square cross-section air bearing, which was used to minimize lateral and rotational motion of the drive shaft. The housing of the air bearing was mounted via leveling screws on an air-supported vibration-isolation table, through which a hole had been drilled to allow passage of the drive column. A rigid aluminum baseplate was mounted on top of the air bearing, and the cell itself was bolted to this plate. An accelerometer mounted on the bottom of the cell was monitored by a computer and used to measure Γ, the amplitude of the acceleration.

Several different sample cells were used. All were evacuated to a pressure of 0.1 Torr to eliminate the effects of air drag. All cells were cylindrical with an aluminum bottom plate. The cell sidewall and top lid were made of Plexiglas. In two of the cells the Plexiglas sidewall was coated with a proprietary antistatic coating [30]. Without the coating, a monolayer of grains tended to stick to the sidewall up to a few grain diameters above the surface of the layer. This monolayer on the sidewall was not present in the cells with antistatic coating. The presence of these grains had a significant effect on the dynamics of the patterns, as discussed below. The cell used for most of the work reported here had a flat bottom plate and a diameter of 14.6 cm. We also used a cell with antistatic walls and a flat bottom plate 13.9 cm in diameter. Another cell had a bottom plate which was flat out to a diameter of 10.0 cm, then sloped upwards to the sidewall with a 2° ''beach;'' the total cell diameter was 14.7 cm. The fourth cell had antistatic walls and a steeper beach; its base was flat to a diameter of 10.7 cm then sloped up at an angle of 10° to a total diameter of 16.5 cm. The cells with a beach were used to reduce the effect of the sidewall on the orientation of the patterns. Finally, a cell with an inverted beach had the same dimensions as the cell with the 10° beach, but with the opposite slope, so that the layer was deeper at the perimeter of the cell than in the center.

The granular material consisted of spherical bronze particles sieved between 150 and 180 μm in diameter; we thus take the particle diameter d to be 165 μm. Apart from sieving, the particles were used as received from the supplier [31]. The depth of the granular layer was determined from the volume of particles making up the layer and the cell geometry.

The patterns that formed in the granular layer were imaged using a digital video camera mounted above the cell. A ring of LEDs encircling the cell slightly above the level of the granular layer was strobed at $f/2$ to illuminate the patterns. As a result, higher regions of the granular layer were illuminated and appear bright, while lower regions are in

shadow and appear dark. The phase of the strobe relative to the drive signal could be adjusted and was normally set to give maximum visual contrast. The digital images were stored on a personal computer and eventually written to CD-ROM for storage and later analysis.

III. RESULTS

A. Cell-filling spirals and targets

1. General properties

In the frequency range of interest in this work, a subcritical bifurcation to a stripe pattern occurs when Γ is increased slowly through Γ_c. The stripes are straight at onset, but as Γ is increased further in a cell with no beach, the stripes tend to orient perpendicular to the cell wall. In a circular cell this boundary condition forces the stripes to become curved. This leads to the presence of sidewall foci and bowed patterns, consisting of two or more sidewall foci with curved stripes which are generally perpendicular to the sidewall. In cells with a beach, the perpendicular orientation at the boundary is less pronounced, but in both cases curvature of the stripes causes spatial variations in the pattern wave number. This can lead to local instabilities in the pattern, resulting in the appearance of defects and time dependence [14]. As a result the steady-state pattern in this regime is predominantly stripelike, but with defects and a continual time dependence.

In the experiments reported here, Γ was increased in a sudden jump from below to above onset. The values of Γ given below are in all cases the final values attained after the jump. In many cases, this jump simply resulted in a stripe pattern with many defects, which annealed over time to a pattern similar to those obtained for a quasistatic increase of Γ, as described above. In a range of frequencies and layer depths, however, large cell-filling spiral or target patterns developed. Examples are shown in Fig. 2. In cells with no beach, these large spirals were observed in layers of depth $N=15.4$, 17.5, and 19.0, but not in runs with $N=13.1$ or smaller. The results in the cells with a beach are somewhat different and will be discussed below.

The range of existence of the cell-filling spirals is shown for $N=15.4$ by the triangles in Fig. 3. Very close to Γ_c we saw no spirals of any kind. Starting a few percent above Γ_c, however, there was a range of f and Γ within which large spirals formed. For this particular depth, large spirals were seen between 29 and 35 Hz, and were most prevalent at 31 and 32 Hz. Large spirals did not appear in every run performed within their range of existence; often stripe patterns with defects formed instead, as described above and illustrated in Fig. 4. Typically, spirals formed more often at frequencies near the middle of their existence range, and were less common at other frequencies. In a somewhat larger range of both Γ and f, not shown in Fig. 3, we observed cases in which the pattern near the edge of the cell initially had the circular symmetry of the cell, as in Fig. 7(b) below, but never developed into a cell-filling spiral. We also saw small, isolated spirals within a mainly stripelike pattern over a much larger range, for Γ all the way up to the transition to hexagons.

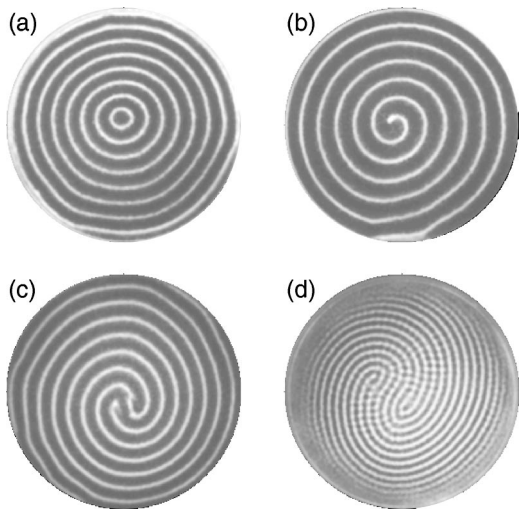

FIG. 2. Examples of cell filling spiral and target patterns. (a) A target pattern; $N=17.5$, $f=32$ Hz, and $\Gamma=2.94$. (b) A one-armed, right-handed spiral; $N=19.0$, $f=29$ Hz, and $\Gamma=2.84$. (c) A three-armed, left-handed spiral; $N=15.4$, $f=32$ Hz, and $\Gamma=3.15$. (d) An 11-armed, left-handed spiral $N=6.7$, $f=35$ Hz, and $\Gamma=2.66$. (a)–(c) were in a circular cell and (d) was recorded in the cell with the 2° beach.

At higher f we observed spiral defect chaos — complex time-dependent patterns containing several small spirals coexisting with stripelike regions [12]. This state, which is similar to that observed in Rayleigh-Bénard convection [27,28] is discussed briefly in Sec. III B below.

As shown in Fig. 2, both right- and left-handed spirals were observed. (For a right-handed spiral, moving along a spiral arm in the counterclockwise sense takes one to the core of the spiral.) 59% of the spirals that formed after a

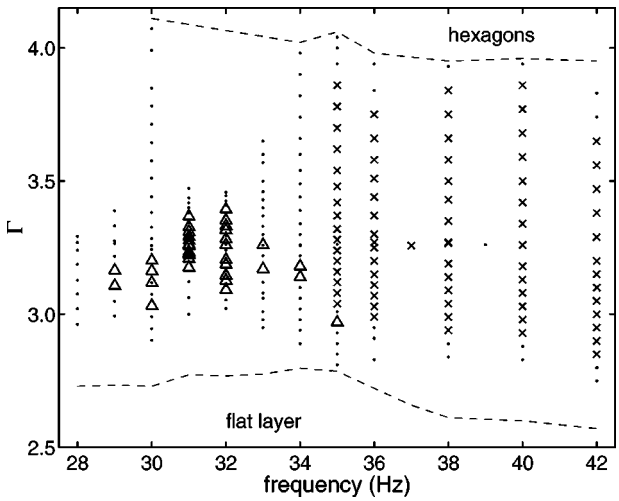

FIG. 3. A diagram showing the range of existence of spiral patterns for $N=15.4$ layers. The lower and upper dashed lines indicate the onset of the stripe pattern at Γ_c and the transition from stripes to hexagons, respectively. The triangles are points at which cell-filling spirals were observed, and the crosses indicate the spiral defect chaos state. Dots indicate other points at which observations were made.

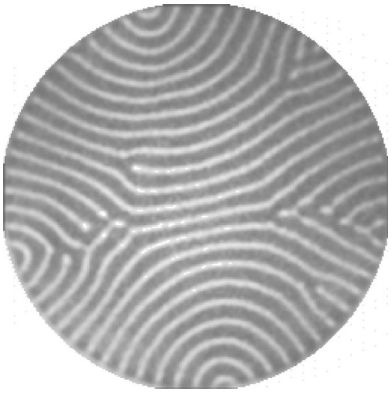

FIG. 4. An example of the type of pattern seen when Γ is increased slowly through onset, or a sufficiently long time after a jump in Γ. This pattern is time dependent, but its predominantly stripelike character and the presence of sidewall foci and other defects are robust features. Here $N=13.1$, $f=35$ Hz, and $\Gamma=3.30$.

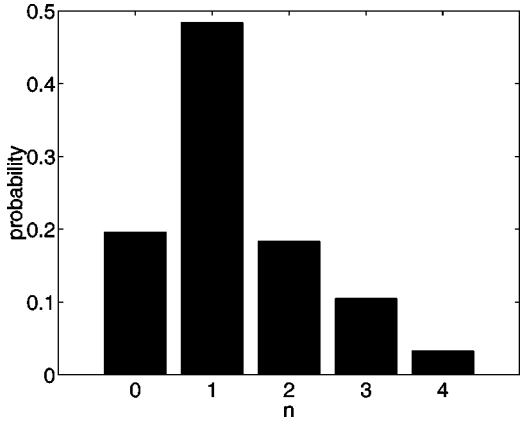

FIG. 5. Histogram of the probability $P(n)$ for the formation of n-armed spirals following a jump in Γ. A total of 154 cell-filling spirals were observed at three layer depths ($N=15.4,17.5,19.0$) for a range of values of Γ and f.

jump in Γ were left handed and 41% were right handed. Spirals with from zero arms (i.e., target patterns) up to nine arms were seen in the cells with no beach, and a short-lived spiral with 11 arms, shown in Fig. 2(d), was observed in a cell with a beach. In some cases the number of arms changed as defects moved through the pattern. Normally the spiral arms extended all the way to the cell wall (except in the cells with a beach, as discussed below), but occasionally an arm was observed to end at a dislocation defect in the cell interior. Figure 5 shows the relative probabilities for the formation of n-armed spirals after a jump in Γ, for runs in the flat-bottomed cells. (Note that these data are only for runs that resulted in the formation of spirals.) Data for all three values of N and many different values of Γ and f are combined in this figure. Only one spiral with $n>4$ was seen in these runs. One-armed spirals were most common, accounting for approximately half of all spirals observed at each depth. No spirals with $n>2$ were observed in the deepest layer studied ($N=19.0$), but otherwise the distribution of n was not strongly dependent on N over the limited range in which the large spirals were observed.

2. Spiral formation

Large spirals typically formed in one of two ways. Figure 6 shows the formation of a target pattern following a jump in Γ from below to about 3.5% above onset. When Γ is increased above onset, a ring forms around the perimeter of the cell. This develops into a pattern of concentric rings as the pattern quickly propagates into the center of the cell from the edge. In the case shown, the end result was a defect-free target. A similar process can lead to the formation of n-armed spirals if one or more defects form in the ring pattern as it develops. The circular cell boundary clearly plays an essential role in this process. The stripe nearest the wall orients parallel to the boundary, in contrast to the tendency towards perpendicular orientation observed when Γ is increased slowly. Interestingly, in a few runs, a target pattern formed first in the center of the cell, then propagated outward to the walls.

A somewhat less clean, but more typical, example of the formation of a spiral pattern is shown in Fig. 7. Starting from a flat featureless layer, Γ is increased from below to 17% above onset. An imperfect circular ring near the cell wall can be seen in Fig. 7(b), but a disordered pattern simultaneously develops in the center of the cell. The pattern close to the wall retains its approximate circular symmetry as the pattern in the interior of the cell gradually anneals and eventually adopts the same symmetry. The end result is a spiral pattern. This process is substantially slower than that shown in Fig. 6, as indicated in the figure captions. If the pattern close to the cell wall develops too many defects or strays too far from circular symmetry the spiral pattern will not form, and instead a stripe pattern with defects results.

3. Dynamics

In the cell with antistatic coating on the wall, the cell-filling spirals rotated uniformly. In the uncoated cell rotation

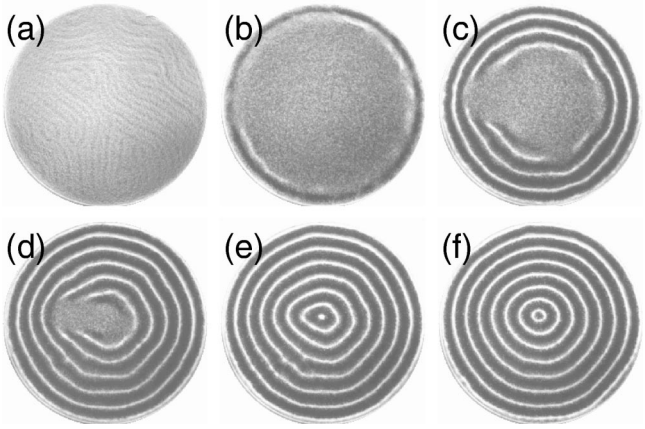

FIG. 6. A time sequence of images illustrating the formation of a target pattern after a jump in Γ from below onset to 2.94. The pattern develops first at the cell wall and propagates in to the center. The remnants of a pattern left over from a previous run can be seen faintly in (a). The elapsed time between (a) and (f) is 6.42 s. $N=17.5$ and $f=32$ Hz.

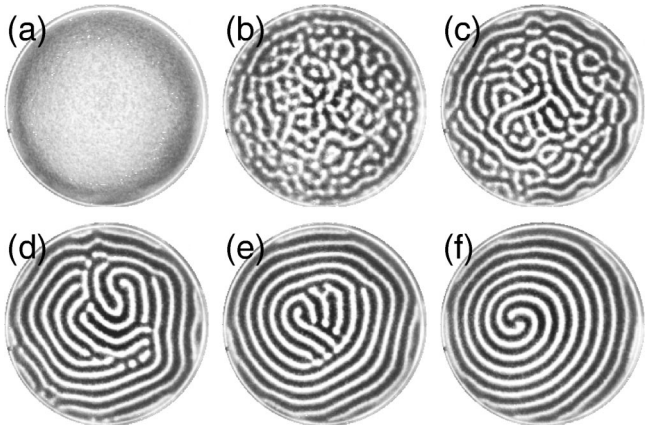

FIG. 7. A time sequence of images showing the formation of a spiral pattern after a jump in Γ from below onset to 3.35. In this case a disordered pattern appears throughout the cell, with a nearly circular ring at the wall. The pattern in the interior of the cell anneals to form a spiral. The time elapsed between (a) and (f) is 39.1 s. Here $N=15.4, f=32$ Hz.

was also observed, but in this case the spirals often became pinned, apparently by the layer of particles adhering to the cell wall due to static. As a result the rotation was not uniform in these cells and in many cases was not present at all. Figure 8 is a sequence of images showing the rotation of a one-armed spiral in the coated cell. Like all spirals in cells with no beach, this one rotated in the direction that ''wound it up.'' This spiral was particularly long-lived and survived intact for 720 s (or 21 000 oscillations of the plate) before eventually drifting off center and being destroyed by the processes described below. Its rotation period was approximately 160 s.

Typical spirals survived much shorter times, usually less than one rotation period. As a result it was not possible to study the rotation rate as a function of the experimental parameters. In general, the spiral core and the outer tips of the arms rotate at similar rates as long as the core is close to the center of the cell. The motion of the core is a combination of rotation and translation (see Sec. III A 4), and as the core translates off center, its rotation rate increases. Meanwhile, the rotation rate of the outer defect at the cell wall can remain steady, decrease slowly, or simply go to zero, depending on the presence or absence of nearby wavelength-changing instabilities of the pattern. As a result, the rotation rate of the spiral is a complicated function of both time and position in the cell.

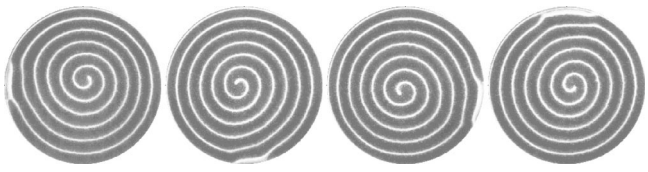

FIG. 8. A time sequence of images showing the rotation of a one-armed spiral. The elapsed time is 139 s, slightly less than one rotation period. Note the rotation of the spiral core as well as that at the cell wall. The spiral rotates in the direction which winds it up. Here $N=19.0$, $f=29$ Hz, and $\Gamma=2.84$.

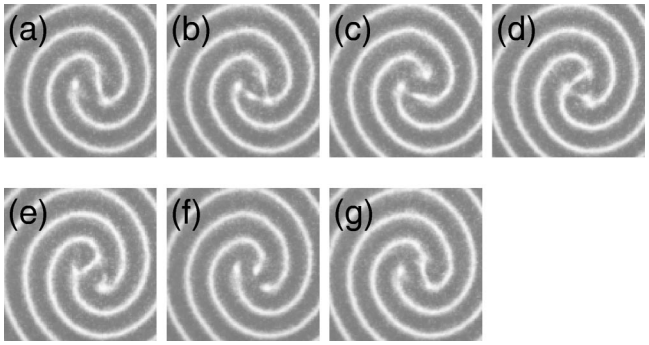

FIG. 9. A time sequence of images showing one period of the core dynamics of a three-armed spiral at $N=15.4$, $f=32$ Hz, and $\Gamma=3.15$. The times of the images are (a) 0 s, (b) 1.83 s, (c) 2.20 s, (d) 2.89 s, (e) 3.58 s, (f) 5.47 s, and (g) 6.17 s.

Interesting dynamics occurred in the cores of the spiral patterns. Examples are shown in Figs. 9 and 10. Figure 9 shows the core of a three-armed spiral. The three bound defects that form the spiral core interact, and the ''bridge'' joining two of the three arms in Fig. 9(a) decays, then reappears between another pair of arms. This behavior repeats with a period that varied somewhat, but on average was 6.1 ± 1.6 s, much faster than the rotation period of the spiral itself. The core of a four-armed spiral is shown in Fig. 10. In this case the period of the core dynamics was more uniform; it was 4.8 ± 0.5 s over the course of this run, but appeared to become larger and more erratic as the core drifted off-center (see below). Similar dynamics were observed in the cores of spirals with different n. The core dynamics illustrated in Figs. 9 and 10 is the same as that observed in cell-filling spirals in Rayleigh-Bénard convection [32–34], as discussed below.

The core of a target pattern also exhibits interesting dynamics, as illustrated in Fig. 11. The phase of the pattern at the core changes continuously, and the core of the target emits circular rings which propagate outwards. A similar process is also seen in Rayleigh-Bénard convection [35]. In our experiments this process is slow when the target core is near the center of the cell — the period is approximately 60 s in Fig. 11 — but as the core drifts off center as described

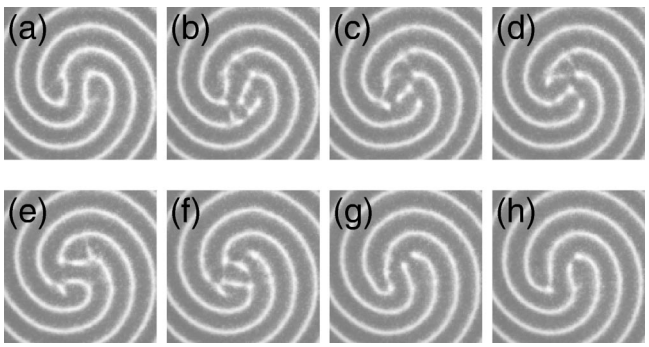

FIG. 10. A time sequence of images showing one period of the core dynamics of a four-armed spiral at $N=15.4$, $f=31$ Hz, and $\Gamma=3.23$. The times of the images are (a) 0 s, (b) 1.10 s, (c) 1.82 s, (d) 2.14 s, (e) 2.86 s, (f) 3.64 s, (g) 4.35 s, and (h) 4.68 s.

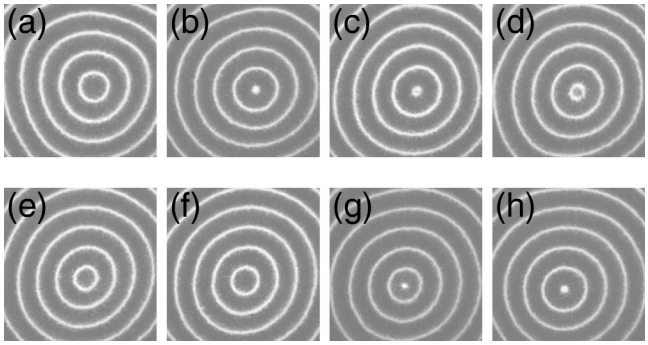

FIG. 11. Time sequence showing dynamics in the center of a target. The times of the images are (a) 0 s, (b) 15.8 s, (c) 31.1 s, (d) 41.5 s, (e) 51.3 s, (f) 61.11 s, (g) 73.3 s, and (h) 81.5 s. $N=19.0$, $f=29$ Hz, and $\Gamma=2.63$.

below the period decreases by a factor of three. In one run the opposite behavior was observed; that is, circular rings propagated in towards the core of the target where they were absorbed.

Instabilities of granular stripe patterns have been discussed in Ref. [14]. Local skew-varicose and crossroll instabilities play an important role in the time dependence of these patterns. Crossrolls in particular are important in the breakup of spiral patterns, as discussed below. We have also observed the oscillatory instability at low frequencies in deep layers. Figure 12 shows an example of an oscillatory instability observed on a spiral pattern in a flat-bottomed circular cell. The same instability has been observed on straight stripes under similar conditions [see Fig. 7(a) of Ref. [12]].

4. Breakup

All of the cell-filling spirals were ultimately unstable in the range of experimental parameters we studied. They typically survived for 1 or 2 min before breaking up. As 1 min corresponds to roughly 2000 oscillations of the plate, or 1000 periods of the subharmonic pattern, these lifetimes are in fact quite long in terms of the characteristic time scale on which energy is injected into the system.

The breakup of the spiral pattern starts with the core of the spiral slowly drifting off center. As a result, the wavelength of the pattern becomes spatially nonuniform, which eventually leads to the development of local instabilities as the wavelength is forced outside of the range in which stripes are stable [14,36]. Examples of this are shown in Figs. 13 and 14. Figure 13 shows a target pattern. The center of the target drifts towards the wall at the bottom left of the figure. The stripes become compressed at the wall at the bottom left and are destroyed by the process illustrated in Fig. 15 and described below. The wavelength of the pattern increases where stripes end at the cell wall as well as on the upstream side of the core. Crossroll instabilities can occur at either of these locations when the local wavelength becomes too large. In Figs. 13(d) and 13(e) crossrolls have appeared where stripes meet the cell walls, as well as at the upper right, where the wavelength has been stretched by the drift of the pattern. These regions become disordered, and in the space of a few seconds the disorder spreads into the rest of

FIG. 12. A one-armed spiral showing an oscillatory instability. This image was taken in a flat-bottomed cell with $N=25$, $f=22$ Hz, and $\Gamma=3.30$.

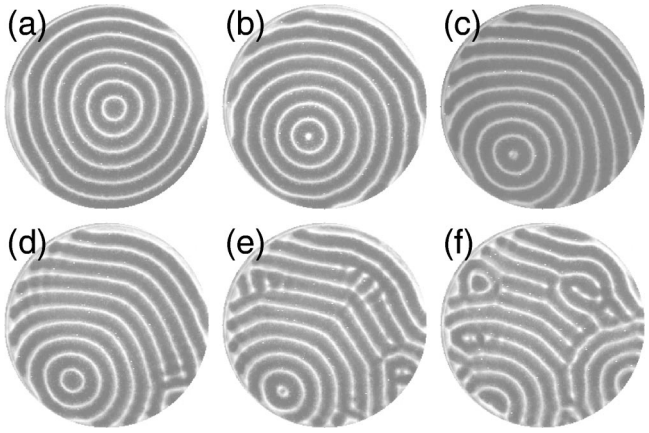

FIG. 13. A time sequence of pictures showing the drift off center and breakup of a target: crossrolls form at the walls where the local wavelength is large. The times of the images are (a) 0 s, (b) 102 s, (c) 126 s, (d) 132 s, (e) 138 s, and (f) 143 s. $N=19.0$, $f=29$ Hz, and $\Gamma=2.63$.

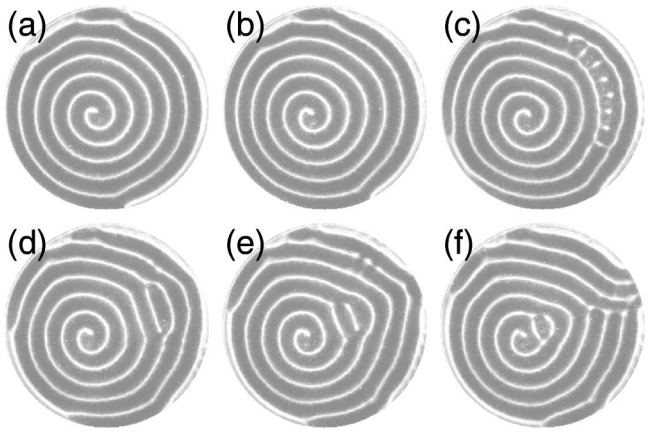

FIG. 14. A time sequence of pictures showing the drift off center and breakup of a spiral: crossrolls form in the interior of the spiral pattern on the ''upstream'' side, again where wavelength is large. The times of the images are (a) 0 s, (b) 4.2 s, (c) 8.5 s, (d) 10.7 s, (e) 12.7 s, and (f) 14.7 s. $N=19.0$, $f=28$ Hz, and $\Gamma=2.79$.

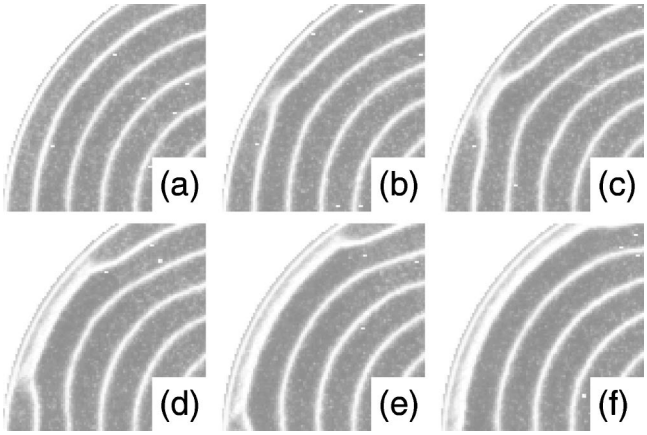

FIG. 15. Time sequence of pictures showing the local destruction of a stripe at the wall. The times of the images are (a) 0 s, (b) 7.3 s, (c) 8.1 s, (d) 10.1 s, (e) 12.1 s, (f) 14.0 s. $N=17.5$, $f=31$ Hz, and $\Gamma=3.45$.

the pattern. In Fig. 13(f) the center of the original target has run into the wall and turned into a sidewall focus. What remains is a disordered stripe pattern with no sign of the original circular symmetry remaining. This process is very similar to that shown in Fig. 21 of Ref. [35] for Rayleigh-Bénard convection. Figure 14 shows a similar scenario, but with crossrolls developing in the interior of the pattern on the upstream side of the core in Fig. 14(c). These crossrolls anneal to form two dislocation defects, which distort the spiral pattern and eventually lead to its destruction both at the wall and in the core, as seen in Fig. 14(f). In all cases the end result of the breakup is a time-dependent stripe pattern with defects similar to that shown in Fig. 4.

As the core of a granular spiral drifts off center, the outermost arm downstream of the core gets pushed closer to the wall. When the arm gets too close to the wall, an instability occurs, as illustrated in Fig. 15. The portion of the spiral arm closest to the wall distorts [Fig. 15(b)] and moves right up to the wall [Fig. 15(c)], where a pair of defects form. These defects then move apart from each other around the cell wall [Figs. 15(d) and 15(e)]. This process appears to be due to a local Eckhaus instability [37] involving the cell wall. One stripe is eliminated locally and the local wavelength is increased, as can be seen by comparing Figs. 15(a) and 15(f). Typically this process repeats several times as the spiral core drifts towards the wall.

5. Wave number evolution

The pattern wave number k changes as the spirals form and evolve in the manner described above. As in Ref. [14], we determined the local wave number using the method introduced in Ref. [36]. An image of the central region of the pattern is band-pass filtered around the fundamental spatial frequency and k is determined as a function of position by taking derivatives of the filtered image [36]. The wave number was then spatially averaged. The spatially averaged wave number $\langle k\rangle$ from one run is shown in Fig. 16. In this particular run, Γ was increased suddenly from below onset to $\Gamma=3.15$ at time $t=0$. The high wave number $\langle k\rangle\sim 6$ observed at small times is that found by our algorithm for the featureless granular layer. The pattern starts at the cell wall and propagates inwards as illustrated in Fig. 6, and as it does so the calculated value of $\langle k\rangle$ decreases steadily. During this time the granular layer is partly patterned and partly flat, and the value of $\langle k\rangle$ we calculate is not characteristic of the pattern itself. However, the pattern fills the cell at approximately the time of the first inset image shown in Fig. 16 (which shows the central region of a circular cell), and beyond this time $\langle k\rangle$ is in fact the mean wave number of the pattern. After the pattern fills the cell, $\langle k\rangle$ continues to decrease steadily as high-spatial-frequency features smooth out. By the time of the second inset image in Fig. 16, at $t=1.3$ s, the pattern is essentially a spiral with several defects. From the second to the third inset ($t=5.0$ s) the decrease of $\langle k\rangle$ continues, but more slowly. The topology of the pattern changes little but the pattern becomes sharper and less noisy. Just before the fourth inset at $t=38.1$ s, the final defects anneal out and we are left with a target pattern. At this point the wave number of the pattern is at its minimum. In the fourth inset this target has started to drift off center, as described above. This drift is accompanied by an *increase* in $\langle k\rangle$. In the last inset ($t=259$ s), the target pattern has broken up completely and we are left with a stripe pattern with defects. The mean wave number of the final stripe pattern is roughly 10% higher than that of the target pattern which preceded it.

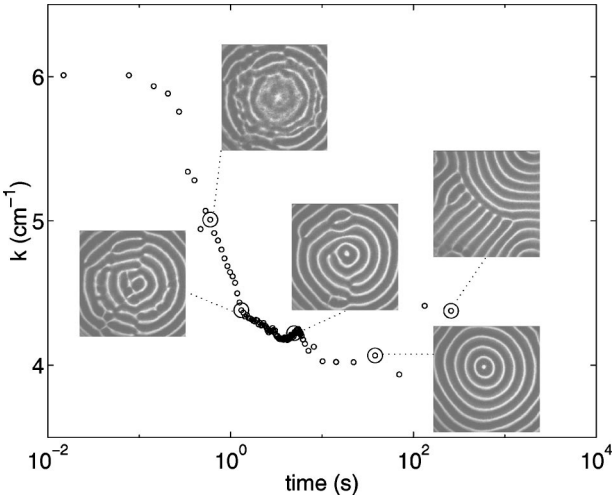

FIG. 16. The mean wave number of the pattern as a function of time for a run with $N=17.5$, $\Gamma=3.15$, and $f=31$ Hz. Time is plotted on a logarithmic scale for display purposes; $t=0$ corresponds to the time at which Γ was suddenly increased from below onset. The five inset images show the central region of the pattern at the data points indicated by large circles.

The evolution of $\langle k\rangle$ described above and shown in Fig. 16 is typical of that observed in several runs. Much the same behavior was observed independent of whether a spiral pattern formed or not, although it was not possible to identify a consistent functional form for the time dependence of $\langle k\rangle$ [38] from our data. In particular, the final increase in wave number also occurred in runs where no spiral pattern formed. This increase appears to be associated with the formation of

FIG. 17. A snapshot of the spiral defect chaos state in a flat-bottomed cell at $N=15.4$, $f=40$ Hz, and $\Gamma=3.13$. This pattern is time dependent and eventually evolves to a stripe pattern with defects as in Fig. 4.

focus defects at the cell sidewall [28], which evidently select a higher wave number than that preferred in their absence.

B. Spiral defect chaos

As shown in Fig. 3, a spiral defect chaos state is observed for frequencies higher than those for which cell-filling spirals occur. In this region the pattern that develops after a jump in Γ consists of several small spirals along with stripelike regions and other defects. These patterns are time dependent. As with the cell-filling spirals discussed above, the spiral defect chaos is a transient and the patterns eventually evolve to a stripe pattern with defects.

A snapshot of the spiral defect chaos state is shown in Fig. 17. This figure shows several small sidewall foci around the perimeter of the cell, and a collection of six small zero- and one-armed spirals in the interior. Most of the small spirals seen in this state had either zero or one arm, but the number of spirals and their handedness varied from run to run.

C. Cells with a beach

The beach geometry used in some experiments modified the boundary conditions at the cell perimeter. For sufficiently thin layers, the patterns formed in the center of the cell and did not extend all the way to the cell wall. For layers with $N \gtrsim 2$ at the edge, the patterns filled the entire cell, but the tendency for the stripes to orient perpendicular to the walls was reduced by the beach, particularly for the thinner layers.

In the cell with the shallow (2°) beach, no large spirals were seen for the values of N which produced large spirals in the flat-bottomed cells. On the other hand, large spirals were observed in this cell with thinner layers. An example of a spiral with 11 arms observed with $N=6.7$ in the center of this cell is shown in Fig. 2(d). In this case the layer is only 1.8 particles deep at the cell wall and the pattern does not fill the cell. This spiral lasted in the form shown for only about 10 s. Crossrolls continually developed over much of its core, as can be seen in Fig. 2(d), and led to changes in the number

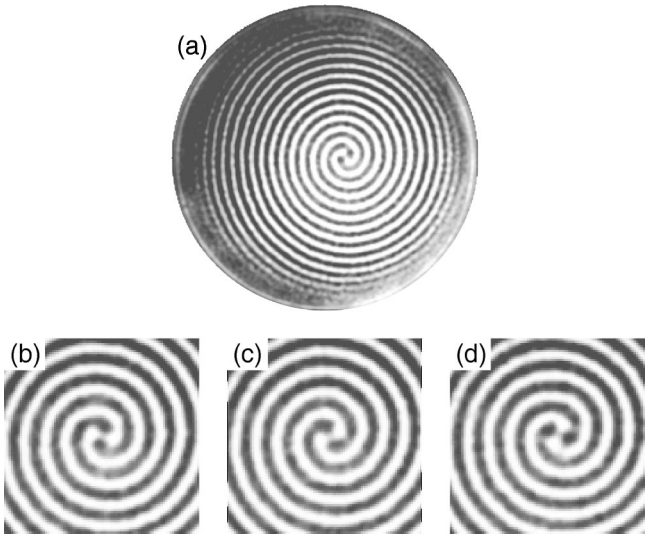

FIG. 18. A time sequence of images showing the rotation of a two-armed spiral in the cell with the 2° beach. Here $N=6.7$ in the center of the cell, $f=35$ Hz, and $\Gamma=2.81$. Image (a) shows the entire cell at time 0 s. (b)–(d) show the core of the spiral at times 9.8, 19.5, and 29.3 s. The spiral does not extend all the way to the cell wall because of the beach. Note that the spiral rotates in the unwinding direction, in contrast to the case in the flat-bottomed cell shown in Fig. 8.

of arms on a time scale of a few seconds. In the cell with the steeper (10°) beach, large spirals were seen at a depth of $N=17.5$ for f from 22 Hz to 35 Hz, and at $N=11$ for f in the range 30–35 Hz, but none were observed for $N=7$.

The lifetimes of spirals in the cells with the 2° and 10° beaches were on the order of only 10 s, substantially shorter than in the flat-bottomed cells. The spirals decayed by moving off-center towards the cell walls, and then evolving to a disordered stripe pattern. Typically, however, a new large spiral would then *spontaneously* reform and the process would repeat. In the cell with the inverted beach, stripes always formed perpendicular to the sidewall and cell-filling spirals were not observed.

A two-armed spiral in the cell with the 2° beach is shown in Fig. 18. Examination of the core of this spiral in Fig. 18(b)–18(d) shows that it rotates in the *unwinding* sense, that is, in the opposite direction to those in the flat-bottomed cells. This reverse rotation was always observed in the cells with a beach. In the flat-bottomed cell the rotation of the spiral was accompanied by the motion of the ends of the spiral arms around the cell perimeter, as in Fig. 8, but here the spiral arms do not reach the cell wall. The outer regions of the spiral appear not to change over the rotation period of the spiral shown in Fig. 18; in particular, the arm which dies away at approximately the 3 o'clock position in Fig. 18(a) continues to do so, independent of the orientation of the spiral core.

IV. DISCUSSION

We observe large spirals developing when Γ is increased suddenly from below to above Γ_c. For flat-bottomed circular

cells, spirals appear in deep layers ($N \gtrsim 13$), in a region where stripes are the stable pattern when Γ is increased quasistatically. These cell-filling spirals are simply stripes that are wound up, and whether stripes or spirals are observed depends strongly on the effect of the boundary conditions at the cell wall.

Smaller spirals within a larger stripelike pattern form in the same frequency range over essentially the whole range of Γ, all the way up to the transition to hexagons.

For all experimental conditions we have studied, the cell-filling spirals are transients. They form either by propagation of a circularly symmetric pattern in from the sidewall or by the annealing of the disordered central region of the pattern in the presence of a circularly symmetric pattern at the cell wall. During this stage of the pattern's evolution, its mean wave number $\langle k \rangle$ decreases, approaching a constant value as the defects anneal. The spirals survive for of order 1000 oscillations of the bottom plate. The core of the spiral then drifts slowly off center, leading to distortions of the pattern's wave number field and eventually to the disruption of the pattern by the crossroll instability in regions where the local pattern wavelength is large. Once the spiral symmetry is disrupted, the pattern fairly quickly evolves to a time-dependent stripe or bowed pattern with defects, similar to those obtained in quasistatic experiments. The mean wave number $\langle k \rangle$ increases during this process as sidewall foci form and the pattern becomes stripelike.

In the cells with a beach, large spirals were observed in thinner layers, for which the boundary conditions allowed the stripes to orient parallel to the sidewall. These spirals were also transients, but in this case spirals would break up, then spontaneously reform, in contrast to what happens in the flat-bottomed cells.

Cell-filling spirals and target patterns have been observed in experiments on the Faraday instability with high-viscosity fluids [29]. They formed when Γ was increased suddenly through the pattern onset, as in the present case, and persist for the duration of the experiment.

Similar large spirals have also been observed in Rayleigh-Bénard convection experiments [28,32,33,39–41]. In Rayleigh-Bénard convection the flow pattern is driven by a temperature difference applied across a fluid layer. Spiral or target patterns are observed in circular cells in the presence of thermal forcing by the cell sidewalls [35,42]. Static sidewall forcing can occur as a result of lateral temperature gradients near the walls, while transient forcing occurs when the temperature difference is suddenly changed. Convection rolls align perpendicular to the sidewalls in the absence of sidewall forcing, and the effect of the forcing is to cause the rolls to align parallel to the walls.

Target patterns ($n=0$ spirals) in convection have been studied experimentally by Hu *et al.* [35], as well as by several other groups [32,33,43–46]. In the presence of well-characterized static sidewall forcing, Hu *et al.* [35] found that target patterns were stable at onset and up to a certain value of the reduced control parameter, ϵ. Above that value of ϵ, the targets become unstable to the so-called focus instability [45,47], which causes the core of the target to drift off center. Beyond this instability the behavior of the target varies depending on experimental conditions. Under some conditions, the core of the target continues to drift off center, eventually reaching the wall. Under other conditions, the core periodically emits traveling convection rolls [35]. The distortion of the pattern due to the drift of the target core can lead to local wave number changing instabilities, which can restabilize the core [44,45]. In other cases, a periodic oscillation of the position of the core is observed [33].

Although we have not observed stable target patterns, we have seen in the granular system some similarities to target patterns in convection. In particular, the first stage in the decay of an initially symmetric target pattern is the drifting off center of the core, as in Fig. 13. The emission of traveling stripes from the target core was also observed, as shown in Fig. 11. We also observed the absorbtion of stripes by the core; to our knowledge this process has not been observed in convection experiments. In convection the drift of the core and the emission of stripes are both accompanied by a large scale mean flow in the fluid layer [35,46,48]; presumably a similar large scale granular flow occurs in the granular system. We do not see the target pattern restabilizing as a result of wave number adjustments away from the core; in our case local instabilities tend to destroy the circular symmetry of the pattern.

Cell-filling spirals with $n>0$ have been studied in convection experiments by several groups [27,32,33,39,40]. Again it is found that large spirals develop in the presence of sidewall forcing, and are stable at low ϵ. The spirals rotate in the winding-up direction, and the n spiral arms end at n dislocation defects in the interior of the cell; outside of these defects the pattern consists of concentric rolls [32,33,39,40]. Above a certain value of ϵ the spiral core moves off center. This drift causes local variations in the wave number of the pattern, and eventually the pattern becomes unstable to the skew varicose instability where it is most compressed. This leads to the appearance of defects which migrate through the pattern, leading eventually to a spiral pattern with a different n, a bowed pattern, or spiral defect chaos. Large spirals in convection have been studied theoretically by several groups [49–51].

There are both similarities and differences between the behavior of large spirals in the granular system and those observed in Rayleigh-Bénard convection. In the absence of pinning at the walls, the granular spirals in the flat-bottomed cells rotate in the winding-up sense. In the cells with a beach, however, they rotate in the opposite sense. In convection, the spiral arms end at defects in the interior of the cell, but in the granular case the arms almost always ended at the cell wall. In both cases the breakup of a spiral starts with its core moving off-center and distorting the wave number field of the pattern. In convection, the skew varicose instability develops where the wave number is large. In the granular case, in contrast, we usually observe the crossroll instability in regions where the local wave number is too small, as well as the wall-mediated instability shown in Fig. 15.

The fast dynamics observed in the spiral cores in our experiments and in convection appears to be the same. For example, our Figs. 9 and 10 can be compared directly with

Figs. 9 and 11 of Ref. [32]. Core dynamics in large spirals has been studied theoretically in Ref. [52], and simulations done for the convection system [28] suggest that the core dynamics in that case results from a mean flow in the spiral core which couples the tips of the spiral arms.

In convection, spirals are stabilized by sidewall forcing, and sidewall forcing must also play a role in the granular case. The role of the forcing, as in convection, is to orient the stripes parallel to the cell wall, and so impose the circular geometry of the cell on the pattern formation process. This was illustrated in Figs. 6 and 7. In the granular system, however, the sidewall forcing in the flat-bottomed cells appears to be transient and the spirals eventually decay to patterns in which stripes preferentially orient perpendicular to the sidewall. In this case, the (transient) forcing mechanism is strong enough to produce spirals only in deep layers. In the cells with a beach, the forcing is continuous, since it is caused by the slope of the cell bottom plate, and produces spirals in thinner layers. The fact that large spirals continuously die out and reform in the cells with a beach suggests that although the forcing is not transient in this case, it is not strong enough to completely stabilize that spirals.

The source of forcing in our experiments is probably a radially oriented convective flow of the granular material near the side wall. In the cells with a beach, such a flow arises due to the cell bottom geometry, with a radial length scale determined by the length of the beach. Since this process depends only on the cell geometry, it will be continuous as long as the cell is oscillating. In the flat-bottomed cells, the convection is driven by friction between the granular particles and the sidewall — particles next to the sidewall experience a drag force different from those in the bulk of the layer. This effect is strongest when the amplitude of the oscillation is suddenly changed, then dies out as the particles near the wall adjust. The radial extent of this flow is determined by the appropriate length scale for dissipation within the layer.

Knight *et al.* have studied convection driven by sidewall friction in vertically-shaken granular systems [53]. They found that the direction of flow at the sidewalls depended on the wall geometry as well as on the friction coefficient. In particular, in a container with a vertical cylindrical wall they observed downflow next to the wall and upflow in the cell center, while in a conical cell — with a wall slope analogous to that of the cell bottom in our cells with a beach — they observed upflow at the wall and downflow in the center. Downflow at sidewalls with friction has also been observed in numerical simulations.

The fact that spirals rotate in the winding-up sense in flat-bottomed cells but in the unwinding sense in cells with a beach suggests that the convective flows near the boundaries may be in the opposite directions in the two cases. Direct observation, however, indicates that in both the flat-bottomed cells and in the cell with the 10° beach there is a flow of particles radially outwards along the top surface of the granular layer. Thus while this radial flow certainly affects the boundary conditions of the layer and influences the formation of spirals, the details remain unclear.

The spiral defect chaos state observed at high frequencies (Fig. 17) is very similar in appearance to that studied in Rayleigh-Bénard convection [27,28,51,54–59]. Spiral defect chaos exists over a large range of f and Γ in our granular system, but is always a transient that anneals to a stripe pattern with defects as in Fig. 4 [12]. A similar transient spiral-defect chaos state has been observed in convection experiments in a fluid with Prandtl number $\sigma \sim 4$ [57], while for lower values of σ this state was stable in convection [27], and for higher σ it does not appear [54].

In convection, the Prandtl number σ, which is the ratio of the fluid's viscosity to its thermal diffusivity, plays a key role in the formation of spiral patterns, since it is easier for mean flows to produce curvature in the convection pattern in fluids with small σ. Coupling between mean flows and curvature occurs in other systems as well [60]. It has been demonstrated in simulations [14] that mean flows couple to the pattern in oscillated granular layers in the same way as in fluids. The existence of large spirals, the observed tendency for small spirals to form even outside of the range in which cell-filling spirals are observed, and the fact that curved stripes and sidewall foci are common in steady-state patterns, all suggest that the coupling between mean flows and the pattern is relatively strong in the range of experimental parameters that we have studied.

V. CONCLUSIONS

We have observed large, cell-filling spirals in vertically oscillated granular layers. These transient patterns exist over a range of parameters within the region where stripe patterns are stable. The formation of large spirals depends strongly on the boundary conditions at the cell sidewall. In cells with a beach (for which the depth decreases with radial position in a ring near the cell wall), unstable spirals that rotate in the unwinding sense form and decay continuously. In flat-bottomed cells, spirals form after a jump in Γ from below to above onset. They rotate in the winding-up sense and decay over time to stripe patterns with defects. Stripes normally orient perpendicular to the cell wall in the granular system, but spirals form when the boundary conditions at the cell wall are modified by convective flow of the granular material, driven by the bottom plate geometry in the case of cells with a beach, or by friction at the wall for the flat-bottomed cells.

Although some differences have been noted above, the properties and dynamics of these large spirals are generally strikingly similar to those seen in Rayleigh-Bénard convection experiments. The role of sidewall forcing is also the same. Such similar behavior in such physically different systems illustrates the universality of the pattern formation process.

Patterns with strong curvature, spiral defect chaos, and the oscillatory instability are all observed at low Prandtl number in fluid convection, where coupling between curvature in the pattern and mean flows is strong. Our observations suggest that a similar coupling plays an important role in the dynamics of our granular system.

Several other results from this work warrant more detailed experimental or numerical study. These include the sidewall forcing and the mechanism by which it influences the pattern formation; the evolution of the pattern and in particular of its wave number after its initial formation; the dynamics of the spiral defect chaos state; and the development and influence of mean flows in the granular layer on the pattern and its dynamics.

ACKNOWLEDGMENTS

We are grateful to C. Bizon, D. Goldman, W. D. McCormick, B. B. Plapp, J. B. Swift, and S. W. Morris for helpful discussions. This research was supported by the Engineering Research Program of the U.S. Department of Energy Office of Basic Energy Sciences, and the Natural Sciences and Engineering Research Council of Canada.

[1] H. M. Jaeger, S. R. Nagel, and R. B. Behringer, Rev. Mod. Phys. **68**, 1259 (1996).
[2] L. P. Kadanoff, Rev. Mod. Phys. **71**, 435 (1999).
[3] S. Fauve, S. Douady, and C. Laroche, J. Phys. (Paris), Colloq. **50 C3**, 187 (1989); Europhys. Lett. **8**, 621 (1989).
[4] B. Thomas, M. O. Mason, Y. A. Liu, and A. M. Squires, Powder Technol. **57**, 267 (1989).
[5] F. Melo, P. Umbanhowar, and H. L. Swinney, Phys. Rev. Lett. **72**, 172 (1994).
[6] F. Melo, P. B. Umbanhowar, and H. L. Swinney, Phys. Rev. Lett. **75**, 3838 (1995).
[7] S. Luding, E. Clément, J. Rajchenbach, and J. Duran, Europhys. Lett. **36**, 247 (1996).
[8] E. Clément, L. Vanel, J. Rajchenbach, and J. Duran, Phys. Rev. E **53**, 2972 (1996).
[9] P. B. Umbanhowar, F. Melo, and H. L. Swinney, Nature (London) **382**, 793 (1996).
[10] P. B. Umbanhowar, Ph.D. thesis, University of Texas at Austin, 1996 (unpublished).
[11] T. Metcalf, J. B. Knight, and H. M. Jaeger, Physica A **236**, 202 (1997).
[12] P. B. Umbanhowar, F. Melo, and H. L. Swinney, Physica A **249**, 1 (1998).
[13] C. Bizon, M. D. Shattuck, J. B. Swift, W. D. McCormick, and H. L. Swinney, Phys. Rev. Lett. **80**, 57 (1998).
[14] J. R. de Bruyn, C. Bizon, M. D. Shattuck, D. Goldman, J. B. Swift, and H. L. Swinney, Phys. Rev. Lett. **81**, 1421 (1998).
[15] P. K. Das and D. Blair, Phys. Lett. A **242**, 326 (1998).
[16] P. B. Umbanhowar and H. L. Swinney, Physica A **274**, 345 (2000).
[17] C. Bizon, M. D. Shattuck, J. R. de Bruyn, J. B. Swift, W. D. McCormick, and H. L. Swinney, J. Stat. Phys. **93**, 449 (1998).
[18] L. S. Tsimring and I. S. Aranson, Phys. Rev. Lett. **79**, 213 (1997).
[19] H. Sakaguchi and H. R. Brand, J. Phys. II **7**, 1325 (1997).
[20] T. Shinbrot, Nature (London) **389**, 574 (1997).
[21] E. Cerda, F. Melo, and S. Rica, Phys. Rev. Lett. **79**, 4570 (1997).
[22] D. H. Rothman, Phys. Rev. E **57**, 1239 (1998).
[23] S. C. Venkataramani and E. Ott, Phys. Rev. Lett. **80**, 3495 (1998).
[24] J. Eggers and H. Riecke, Phys. Rev. E **59**, 4476 (1999).
[25] C. Bizon, M. D. Shattuck, and J. B. Swift, Phys. Rev. E **60**, 7210 (1999).
[26] M. D. Shattuck, C. Bizon, J. B. Swift, and H. L. Swinney, Physica A **274**, 158 (1999).
[27] S. W. Morris, E. Bodenschatz, D. S. Cannell, and G. Ahlers, Phys. Rev. Lett. **71**, 2026 (1993); Physica D **97**, 164 (1996).
[28] E. Bodenschatz, W. Pesch, and G. Ahlers, Annu. Rev. Fluid Mech. **32**, 709 (2000).
[29] W. S. Edwards and S. Fauve, J. Fluid Mech. **278**, 123 (1994).
[30] SC Technologies, Amarillo, TX; http://www.sctech.com.
[31] ACuPowder, Union, NJ; http://www.acupowder.com.
[32] B. B. Plapp and E. Bodenschatz, Phys. Scr. **T67**, 111 (1996).
[33] B. B. Plapp, Ph.D. thesis, Cornell University, 1997 (unpublished).
[34] M. Assenheimer, Ph.D. thesis, Weizmann Institute, Rehovot, Israel, 1994 (unpublished).
[35] Y. Hu, R. Ecke, and Phys. Rev. E **48**, 4399 (1993); Phys. Rev. Lett. **72**, 2191 (1994).
[36] D. A. Egolf, I. V. Melnikov, and E. Bodenschatz, Phys. Rev. Lett. **80**, 3228 (1997).
[37] W. Eckhaus, *Studies in Nonlinear Stability Theory* (Springer, New York, 1965).
[38] M. C. Cross and D. I. Meiron, Phys. Rev. Lett. **75**, 2152 (1995).
[39] E. Bodenschatz, J. R. de Bruyn, G. Ahlers, and D. S. Cannell, Phys. Rev. Lett. **67**, 3078 (1991).
[40] B. B. Plapp, D. A. Egolf, E. Bodenschatz, and W. Pesch, Phys. Rev. Lett. **81**, 5334 (1998).
[41] A. Pocheau and F. Daviaud, Phys. Rev. E **55**, 353 (1997).
[42] J. R. de Bruyn, E. Bodenschatz, S. W. Morris, S. P. Trainoff, Y. Hu, D. S. Cannell, and G. Ahlers, Rev. Sci. Instrum. **67**, 2043 (1996).
[43] E. L. Koschmieder and S. G. Pallas, Int. J. Heat Mass Transf. **17**, 991 (1974).
[44] V. Croquette, M. Mory, and F. Schosseler, J. Phys. (Paris) **44**, 293 (1983).
[45] V. Steinberg, G. Ahlers, and D. S. Cannell, Phys. Scr. **32**, 534 (1985).
[46] V. Croquette, P. LeGal, A. Pocheau, and R. Guglielmetti, Europhys. Lett. **1**, 393 (1986).
[47] A. C. Newell, T. Passot, and M. Souli, J. Fluid Mech. **220**, 187 (1990).
[48] V. Croquette, Contemp. Phys. **30**, 153 (1989).
[49] M. C. Cross and Y. Tu, Phys. Rev. Lett. **75**, 834 (1995); M. Cross, Physica D **97**, 65 (1996).
[50] X. J. Li, H. W. Xi, and J. D. Gunton, Phys. Rev. E **54**, R3105 (1996).
[51] W. Pesch, Chaos **6**, 348 (1996).
[52] I. Aronson, M. Assenheimer, V. Steinberg, and L. S. Tsimring, Phys. Rev. E **55**, R4877 (1997); L. S. Tsimring, Physica A **249**, 125 (1998).

[53] J. B. Knight, H. M. Jaeger, and S. R. Nagel, Phys. Rev. Lett. **70**, 3728 (1993).
[54] M. Assenheimer and V. Steinberg, Phys. Rev. Lett. **70**, 3888 (1993); Nature (London) **367**, 345 (1994).
[55] H. W. Xi, J. D. Gunton, and J. Viñals, Phys. Rev. Lett. **71**, 2030 (1992).
[56] W. Decker, W. Pesch, and A. Weber, Phys. Rev. Lett. **73**, 648 (1994).
[57] K. M. S. Bajaj, D. S. Cannell, and G. Ahlers, Phys. Rev. E **55**, R4869 (1997).
[58] G. Ahlers, Physica A **249**, 18 (1998).
[59] D. Egolf, I. V. Melnikov, W. Pesch, and R. E. Ecke, Nature (London) **404**, 733 (2000).
[60] A. Davey, L. M. Hocking, and K. Stewartson, J. Fluid Mech. **63**, 529 (1974).